CAL–NO–002 24 May 1990

To: LAr Accordion Group

From: Michel Lefebvre, Monica Pepe, Giacomo Polesello

Subject: LAr Accordion Calorimeter Simulation

This note is a report on a Monte Carlo study of a LAr calorimeter with accordion design. Optimum geometrical parameters are obtained for the construction of a prototype.

Contents

1 INTRODUCTION

The concept of a LAr calorimeter with accordion geometry (see Fig. 1) is presently under study. The main advantages expected from this structure are a fast readout speed and no dead space for signal lines as the cells can form transmission lines from the inside to the outside of the detector.

A Monte Carlo study was performed using the GEANT simulation package. The main goal of this study is to see whether or not good resolution and good response uniformity can be achieved for incident high energy electrons. The simulated geometry is described in section 2. The electric field configuration in the LAr gaps, described in section 3, is a consequence of the geometry. The effect of non-uniformities in the field due to the electrode shape is also studied.

Electromagnetic shower simulations and measurements of the deposited energy in the presence of the electric field are covered in section 4, followed by a section on the simulation results. The final geometrical parameters retained for the construction of a prototype are summarised in section 6.

2 GEOMETRY

2.1 General Considerations

The LAr Accordion Calorimeter (LAC) is composed of lead sheets with accordion shape separated by LAr gaps. Incident particles travel along the Z axis (see Fig. 1) and hit the LAC at $Z = 0$. The readout electrodes are located in the middle of each LAr gap, as can be seen in Fig. 2.

For simulation purposes, the LAC is divided in *stacks* which are composed of *cells*. Each stack is delimited by two consecutive bends. Within a stack, each cell is delimited by two lead sheets. Two stacks of two cells each are shown in Fig. 2. Each lead sheet is in fact composed of a lead core sandwiched between two thin layers of stainless steel glued on the lead for a total thickness (measured perpendicular to the sheet surface) of ϵ_p. In the simulation, the glue is replaced by fibreglass and stainless steel by iron; a composite material is made with a fraction p_p of lead, p_f of iron and the rest of glue, which means that the fine structure of each lead sheet is not simulated. The values $p_p = 0.818$ and $p_f = 0.091$ were used. Each lead sheet is bent with a radius of curvature (measured at the middle of the sheet's thickness) of R_p.

Each readout electrode is composed of copper and kapton, the last one being simulated by fibreglass. As for the lead sheet, a composite material is built with a fraction p_c of copper and the rest of kapton. A value of $p_c = 0.467$ was used. The total thickness of each readout electrode sheet is ϵ_c, and its radius of curvature at the bends is R_c.

In each cell, each of the two LAr gaps has a thickness of ϵ_l. In general, each side of a given LAr gap bend has a different centre of curvature, which implies that the thickness of the LAr gaps is not constant in the bends. This has important consequences for the simulation: standard GEANT volumes cannot be used and the electric field configuration in the LAr gaps must be obtained numerically.

The last two parameters defining the cell geometry are the bend angle θ, measured with respect to the X axis, and the bend to bend length l (see Fig. 2).

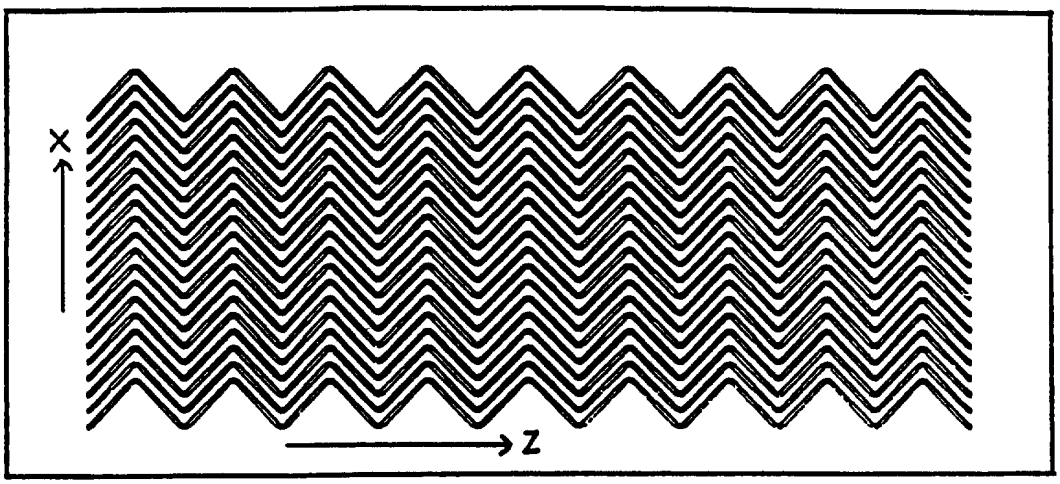

Figure 1: View of the LAC in the $X - Z$ plane, with 18 stacks and 19 cells per stack. Only the lead sheets are shown. Incident particles travel along the Z axis.

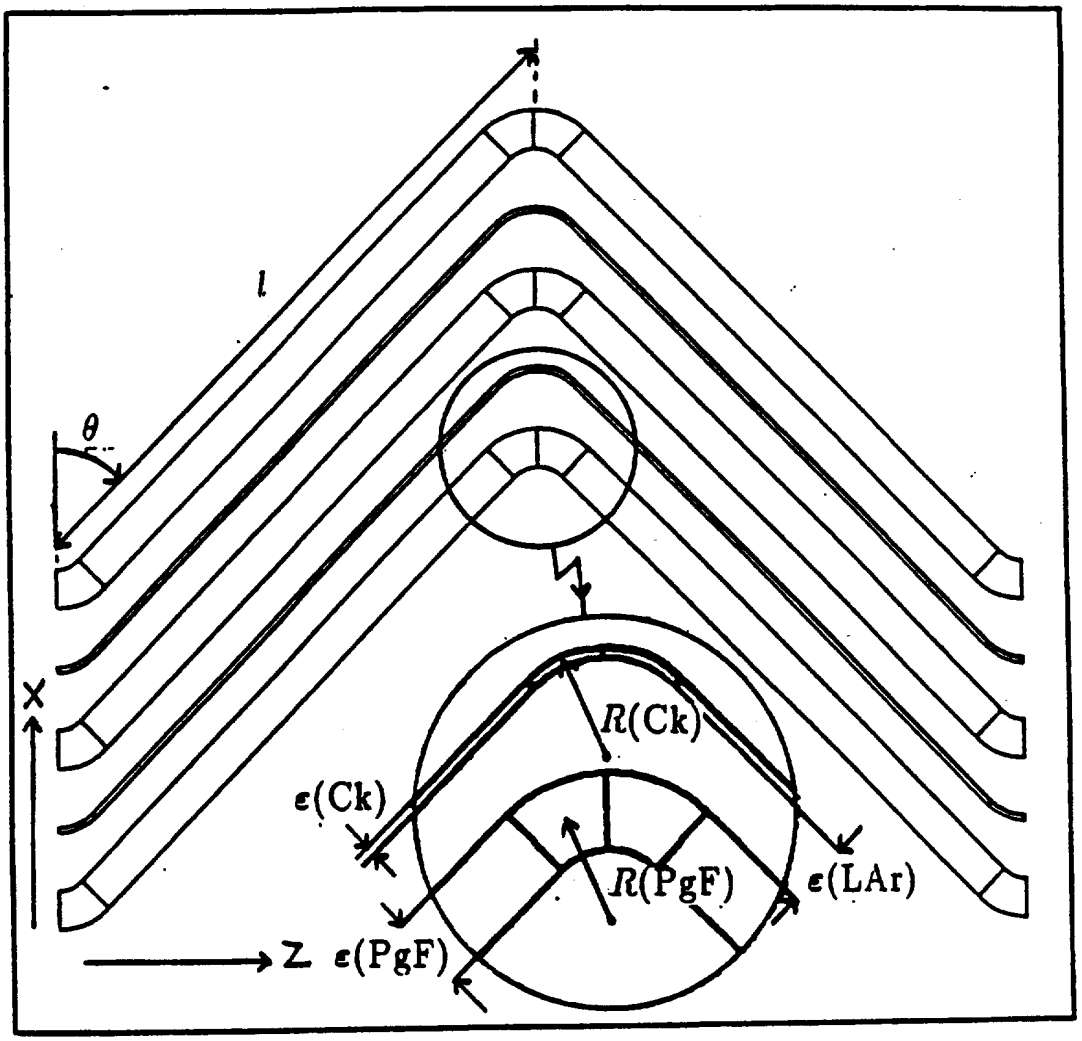

Figure 2: View of four cells in the $X - Z$ plane. The parameters defining the cell geometry are shown.

The total cell thickness is then

$$\epsilon \equiv \epsilon_p + 2\epsilon_l + \epsilon_c.$$

Details of the GEANT implementation of the cell geometry can be found in appendix A.

2.2 Optimum Cell Geometry

In general, the LAr radiation length traversed by a particle travelling in the LAC along the Z axis, and hence the response to this particle, varies as a function of the impact point X value. If the accordion shape had sharp corners, it would be possible to make this LAr radiation length traversed independent of the impact point X value by choosing a set of parameters for which the diffraction relation

$$l\cos\theta = \frac{n\epsilon}{\sin\theta}$$

holds, where n is the number of cells traversed in one stack.

The round corners, mechanically unavoidable and necessary for field smoothness, make things more complicated. Figure 3 shows the variation of LAr radiation length traversed by a particle travelling along the Z axis as a function of the impact X value. The average thickness of LAr is 2.27 radiation lengths (for 18 stacks). The average total thickness traversed is 28.79 radiation lengths. The origin of the X axis is in the centre of the electrode of a given cell at $Z = 0$. In total, two cell widths in X are shown, that is $X \in [-\epsilon/\sin\theta, \epsilon/\sin\theta]$. In Fig. 3, a reasonable set of parameters was empirically optimised. The fluctuations are all contained within the $\pm 5\%$ band. Small departures from this optimum parameter set worsen the uniformity, as can be seen in Fig. 4 where (a) the lead sheet radius of curvature or (b) the LAr gap thickness was modified.

An optimum cell geometry can be obtained approximately from the improved diffraction relation

$$l\cos\theta - 2R_p\left(\frac{1}{\sin\theta} - 1\right) + \frac{\epsilon_p}{2} \approx \frac{n\epsilon}{\sin\theta},$$

but fine tuning must be done empirically.

Figures 3 and 4 are obtained by analytically calculating the LAr radiation length traversed. Since the geometry of the LAr is also known to GEANT through the general simulation program, the same figures can be obtained by simulating the LAC response to muons (see appendix B). The full circles shown in Fig. 4(b) were obtained from a full simulation of the LAC response to muons. The good agreement with the analytic curve provides a strong cross-check of the two methods. Since the analytic method is very fast (a few seconds) and interactive, it is used to quickly optimise the cell geometry. If the angle of incidence departs slightly from zero, the muons response is found to be more uniform as a function of impact point, as shown by open circles in figure 4(b).

The LAC response to electrons must of course be simulated to verify that in the case of an extended shower the best resolution and the best uniformity of response and resolution are also obtained for an optimised cell geometry. The effect of the field non-uniformity and other specificities of charge collection in the calorimeter (shaping) must also be considered.

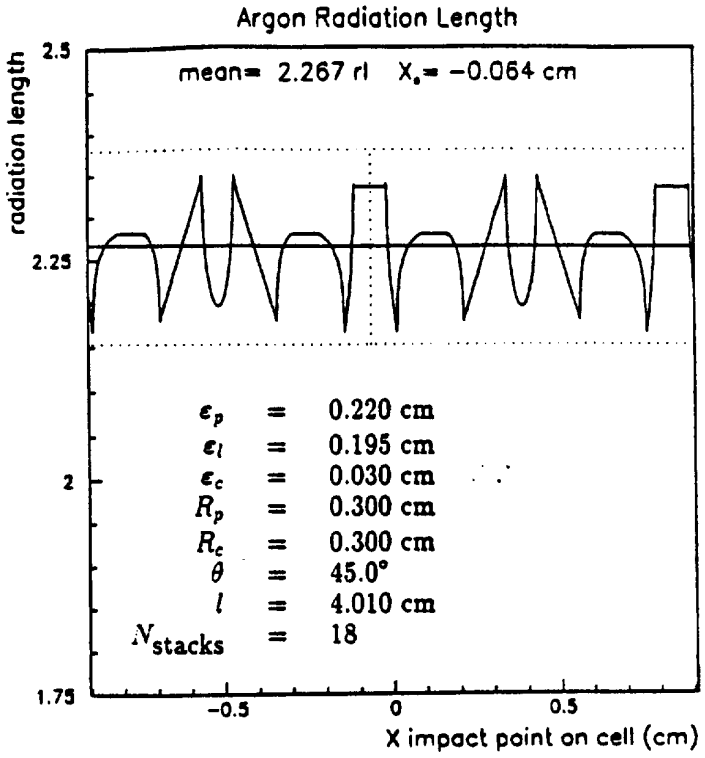

Figure 3: LAr radiation length traversed by a particle travelling along the Z axis as a function of its impact point X value for an optimum cell geometry. The horizontal dotted lines bound a ±5% band.

3 ELECTRIC FIELD

An electric field map was obtained [1] for the cell geometry of Fig. 4(b). A contour plot of the electric field strength for the region of the LAr gaps close to a bend is shown in Fig. 5(a). The readout electrode separating the two LAr gaps is held at $V_o = 2$ kV, while the lead sheets are connected to ground. In the constant field region, the field strength is V_o/ϵ_l, that is 10.53 kV/cm in this case. The field strength goes up to 11.72 kV/cm in the convex bend of the electrode, and decreases to 2.94 kV/cm near the concave bend. Figure 5(b) shows the electric field strength near the Z boundary of a cell.

The electrons from the ionisation of the LAr will drift along the electric field vector, in the opposite direction.

4 ELECTROMAGNETIC SHOWER SIMULATION

The LAC response to electrons was simulated using GEANT version 3.13. The various GEANT parameters used are listed in appendix B.

4.1 Deposited Energy

The GEANT simulation of an electromagnetic shower provides the starting time, the starting point, direction and length of each charged track segment in the LAr, as well

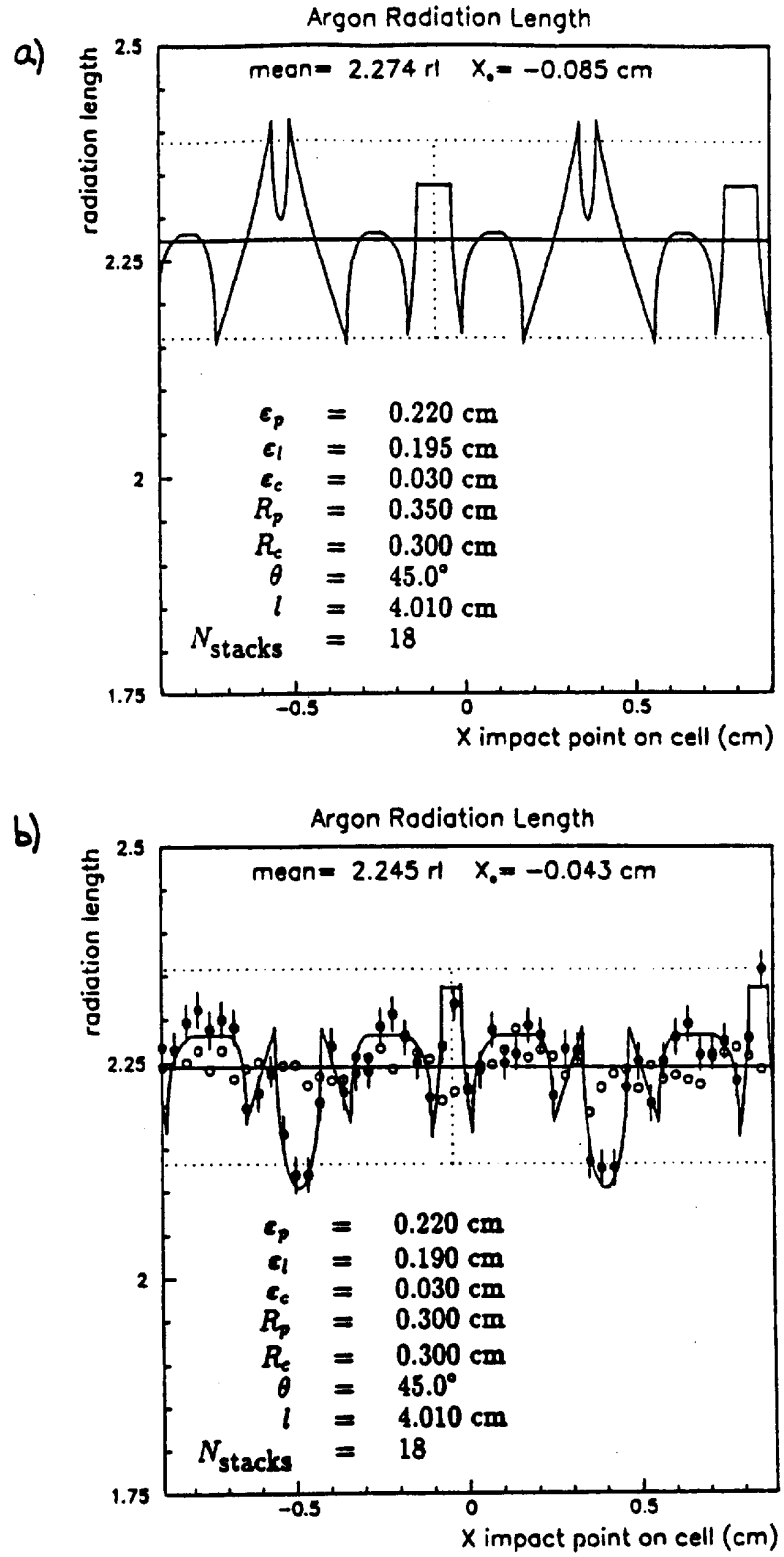

Figure 4: LAr radiation length traversed by a particle travelling along the Z axis as a function of its impact point X value for two non-optimum cell geometries. Compared with an optimum cell geometry, the value of (a) the lead sheet radius of curvature or (b) the LAr gap thickness was changed. The circles are the response obtained by a full simulation of muons impinging on the LAC with normal incidence (full circles) or with 20 mrad incidence angle (open circles). The horizontal dotted lines bound a ±5% band.

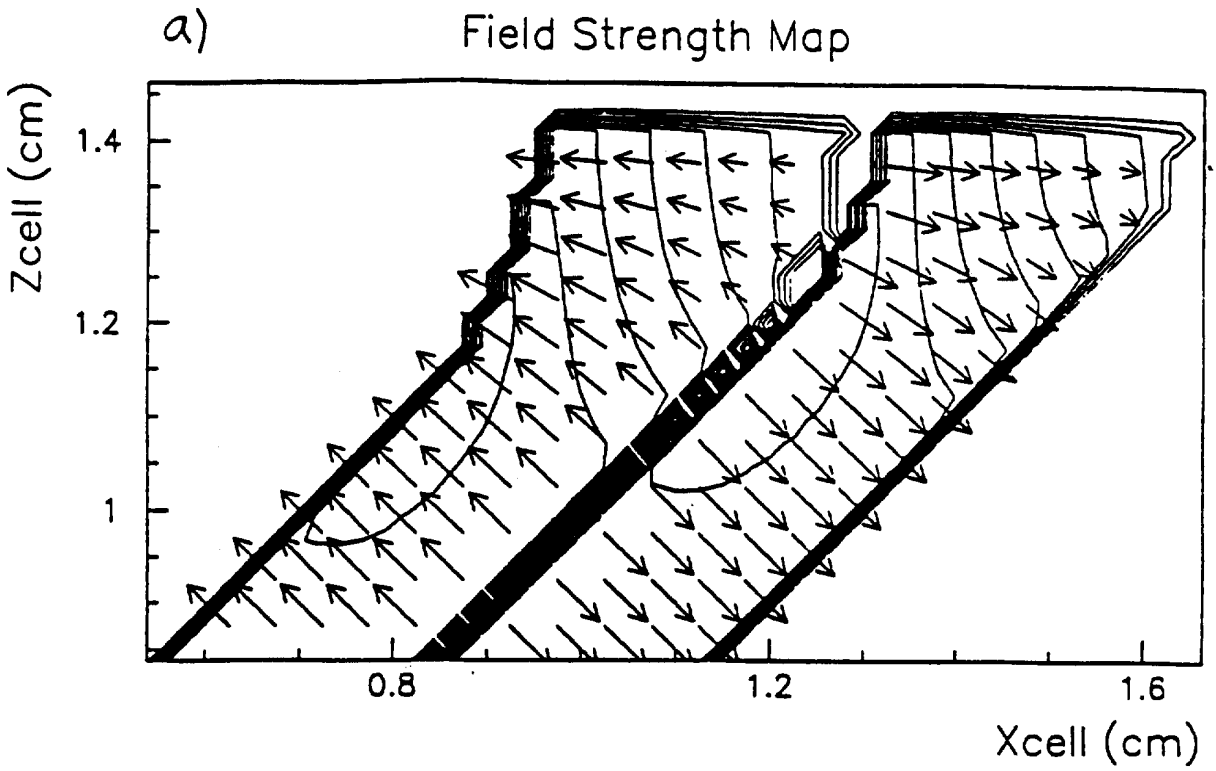

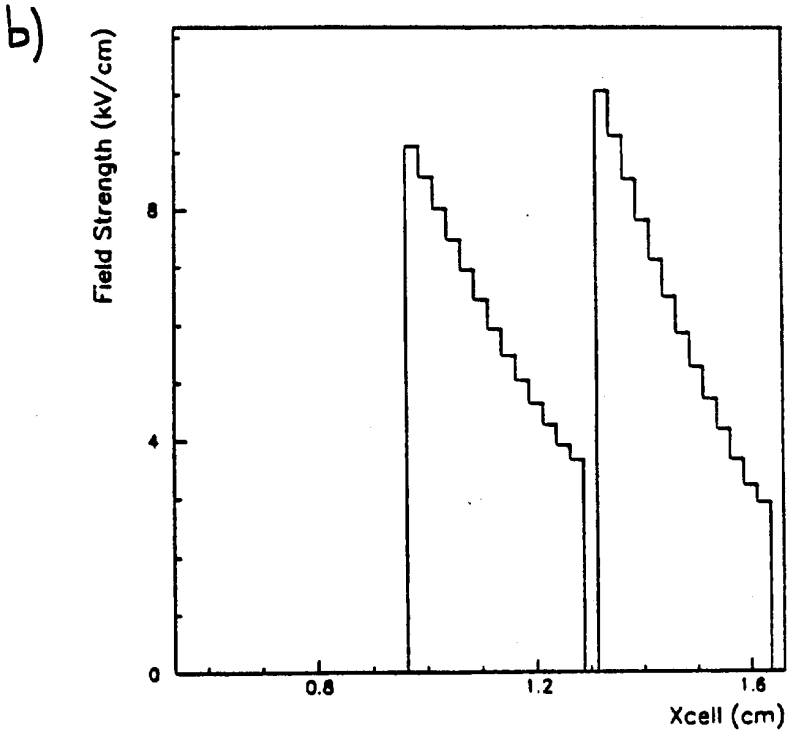

Figure 5: (a) Electric field strength contours for the region of the LAr gaps close to a bend. The field vector is also shown. (b) Electric field strength near the maximum Z value of a cell.

as the associated deposited energy. These quantities associated to each track segment form a *hit*. The electrons and photons are tracked through the LAC down to a cutoff energy of 1 MeV and 100 KeV respectively. Figure 6(a) shows all tracks of a 40 GeV electron shower (the cutoff energy for electrons and photons is here raised to 10 MeV for display reasons). The charged and neutral components can be seen in Figures 6(b) and (c) respectively.

The energy E_i of each of the N hits in a shower can be added to obtain the total energy $E_{\rm tot}$ collected by the LAC

$$E_{\rm tot} = \sum_{i=1}^{N} E_i.$$

For many simulated showers, the distribution of $E_{\rm tot}$ provides the response and the resolution of the LAC, not corrected for charge collection and readout effects.

4.2 Charge Collection and Readout Simulation

Each hit contains the deposited energy E_i, and the associated track segment in the LAr which can be divided in m subsegments. A value of $m = 10$ was used. Assuming that the charges produced in the LAr are distributed uniformly along a given track segment, the total energy collected becomes

$$E^{\rm w}_{\rm tot} = \sum_{i=1}^{N} \sum_{j=1}^{m} w_{ij} E_{ij}$$

where the subsegment energy E_{ij} is given by $E_{ij} = E_i/m$ and w_{ij} is a weight that takes into account the collection and readout of the charge associated to the subsegment j of track segment i.

Let $\vec{x}$ be the position in a cell of the subsegment j of track segment i. The electric field there is $\vec{E}(\vec{x})$, and the drift speed $v(|\vec{E}|)$, for the region of interest, is approximated by [2]

$$v(|\vec{E}|) = a + b|\vec{E}|$$

where $a = 2.3 \times 10^{-4}$ cm/ns and $b = 0.17 \times 10^{-4}$ cm^2/ns/kV. Note that the charge drift is along the electric field vector, in the opposite direction.

The drift of the charge associated to the track subsegment j can then be followed as a function of time. The current distribution is given by

$$I_o(t) \propto \frac{|\vec{E}|v}{V_o}$$

where the electric field and the drift velocity are taken at position $\vec{x}(t)$ and V_o is the electrode voltage (see section 3). The readout electronics is simulated by convoluting the current distribution with the readout electronics time response to a delta function. This response follows a bipolar shape [3] shown in Fig. 7, given by

$$B(t) \propto t^{\beta-1} \left[\beta - \frac{t}{t_{\rm max}}(\beta - \sqrt{\beta})\right] \exp\left[-\frac{t}{t_{\rm max}}(\beta - \sqrt{\beta})\right]$$

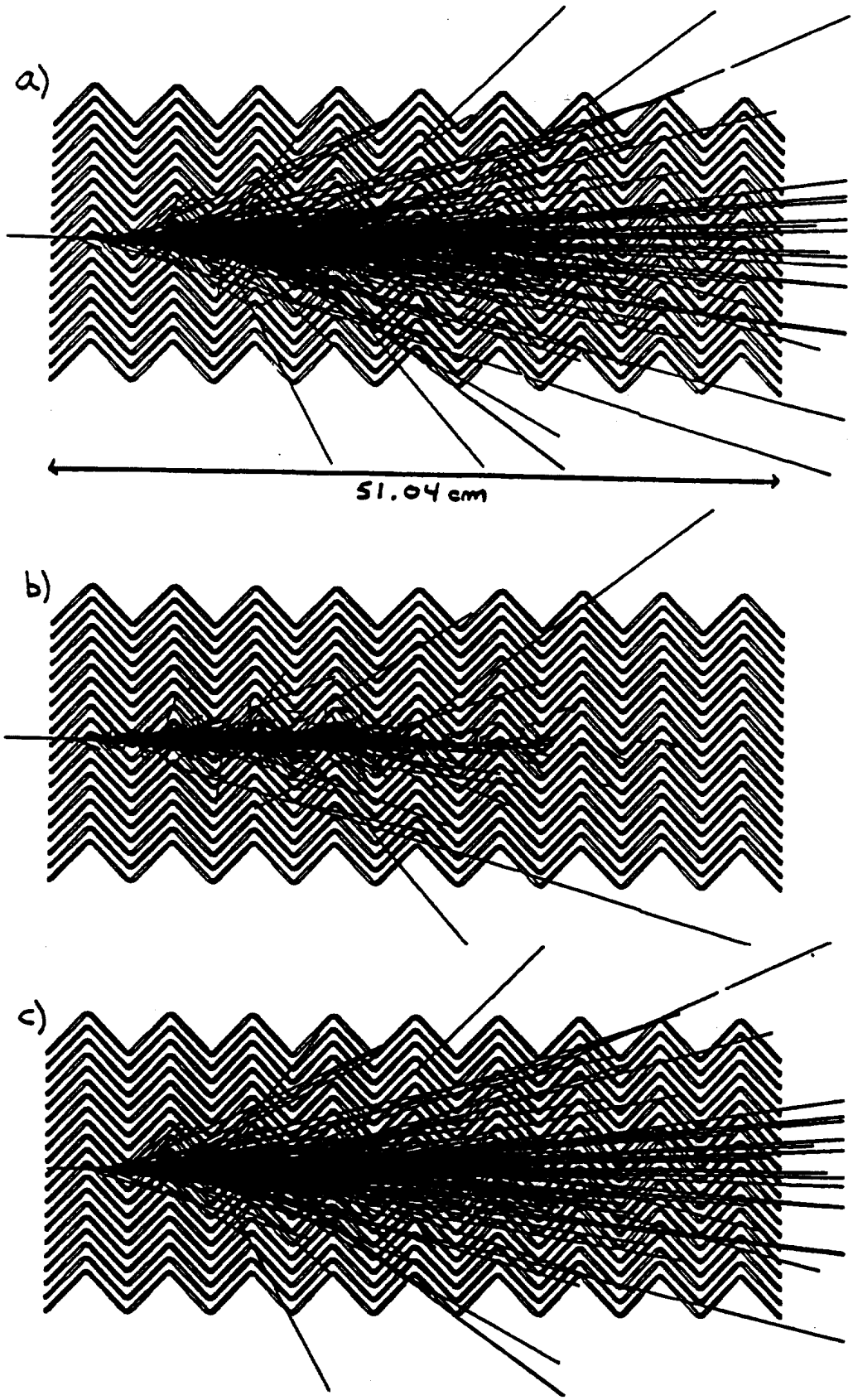

Figure 6: 40 GeV electron shower. All tracks are shown in (a). Only the charged and neutral tracks are shown in (b) and (c) respectively. In these figures, the cutoff energy for electrons and photons is 10 MeV.

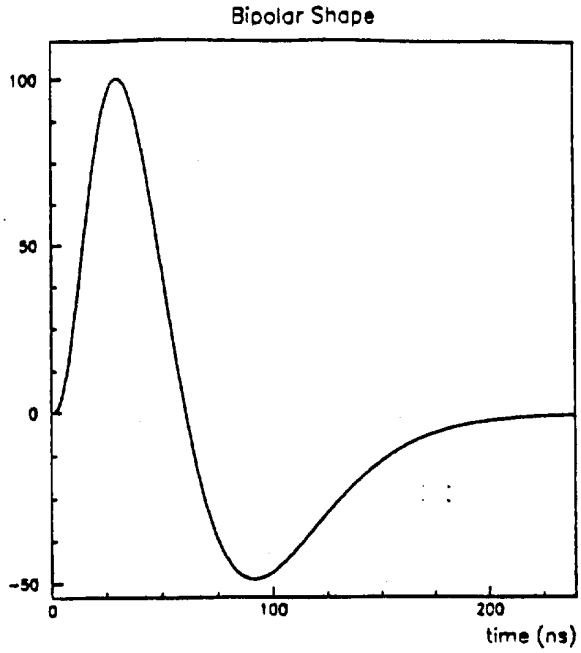

Figure 7: Bipolar shape of the readout electronics response to a step function.

where $\beta = 3.8849$. This bipolar shape is maximum at $t = t_{\max}$, which is set here to 30 ns.

The effective collected current is then

$$I(t) = I_0(t) \otimes B(t) = \int_0^t dt' \, I_0(t') \, B(t - t')$$

since only $0 \leq t' \leq t$ contributes.

The weight w_{ij} is then given by

$$w_{ij} \propto I(t_{\text{sample}})$$

where the sampling time t_{sample} is set to $2t_{\max} = 60$ ns. A charge produced near the readout electrode will contribute little to the total energy because of the sampling time and the convolution with the bipolar shape (readout simulation); a charge produced in a region of high (low) electric field will much (little) contribute to the total energy (charge collection simulation). The weight map therefore follows the electric field map shown in figure 5, except close to the readout electrode where the weights are low. The weights are normalised to 1 in the region of constant electric field, far from the readout electrode.

The electric field available [1] provides a value of $|\vec{E}|$, E_z and E_x every 250 μm. Interpolation or extrapolation in the map is performed to obtain $\vec{E}(\vec{x})$ (see appendix C).

4.3 Computer Time and Space Considerations

The simulation of electron showers in the LAC was performed on the CRAY computer. Approximately 1.72 s/GeV are required for a complete shower simulation, including the writing of hits to tape (this was verified for 20 to 80 GeV electrons). Approximately 5000 hits/GeV are generated within a shower. The effective space (including overheads) of about 57 bytes/hit is needed to store data to tape.

The simulation of a 40 GeV electron shower therefore takes 69 seconds on the CRAY computer. Up to approximately 180 showers can fit on a 200 Mbyte cartridge. In this case, reading back the hits from tape and applying the charge collection and readout correction takes about 7 seconds per shower.

5 RESULTS

The simulation of 40 GeV electrons impinging on the LAC at normal incidence was performed for various impact points. Results on the resolution and response uniformity are presented here, along with preliminary results on the reconstructed shower position.

5.1 Charge Collection and Readout not Simulated

Response and resolution

In the case where the charge collection and the readout are not simulated, results are available for three cell geometries: an optimum cell geometry (as in Fig. 3), and two non-optimum cell geometries where the LAr gap thickness ϵ_l was altered.

For a given geometry, 140 showers were simulated per impact point. The distribution of $E_{\rm tot}$ for 40 GeV electrons hitting an optimum geometry LAC in the centre of a cell is shown in Fig. 8(a). The resolution coefficient

$$\alpha \equiv \frac{\mu}{\sigma}\sqrt{E_o}$$

where μ and σ are respectively the average and r.m.s. of the $E_{\rm tot}$ distribution and $E_o = 40$ GeV is found to be 8.2 ± 0.9 % GeV$^{1/2}$. The fraction of energy deposited in each stack is shown in Fig. 8(b). On average, more than 90 % of the energy is deposited in the first 10 stacks.

The response for various impact points is shown by open circles in Fig. 9 (the average response is adjusted to the LAr radiation length on the figure). The response is also available in table 1, along with the resolution and the resolution coefficient α. It is interesting to note that the response has a 0.86 % r.m.s. over the five impact points probed. Furthermore, the response is found to be above (below) average if the impact point is near the region where an excess (depletion) of LAr is present.

The results for the non-optimum geometries are shown in Fig. 10. The response uniformity in the case of electromagnetic showers is found to be less sensitive to the geometrical parameters of the cell than in the case of muons. The response qualitatively follows the LAr radiation length (or equivalently the muon response). The resolution obtained is comparable to the optimum geometry case, as can be seen in table 1.

Reconstructed shower position

The reconstruction of electromagnetic shower position was studied for 40 GeV electrons at normal incidence on the centre of a cell, for an optimum cell geometry (as in Fig. 3).

To simulate different readout schemes, cells can be taken individually, or grouped in pairs or triplets. For a given cell or cell group, called *supercell*, the energy is summed

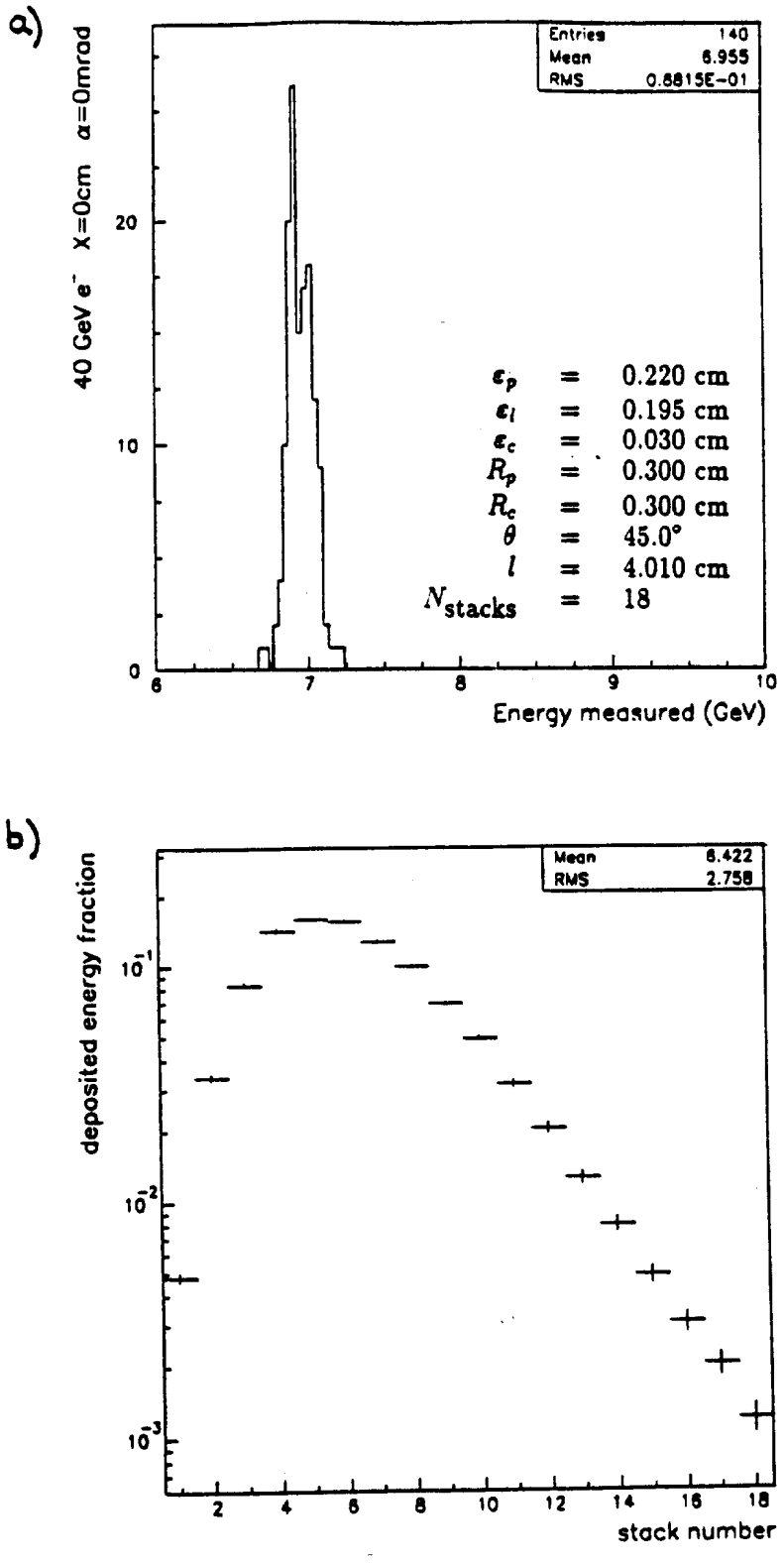

Figure 8: (a) Distribution of the total energy measured for a 40 GeV electron at normal incidence in the centre of a cell for an optimum geometry and (b) the fraction of energy deposited in each stack. The charge collection and readout are not simulated.

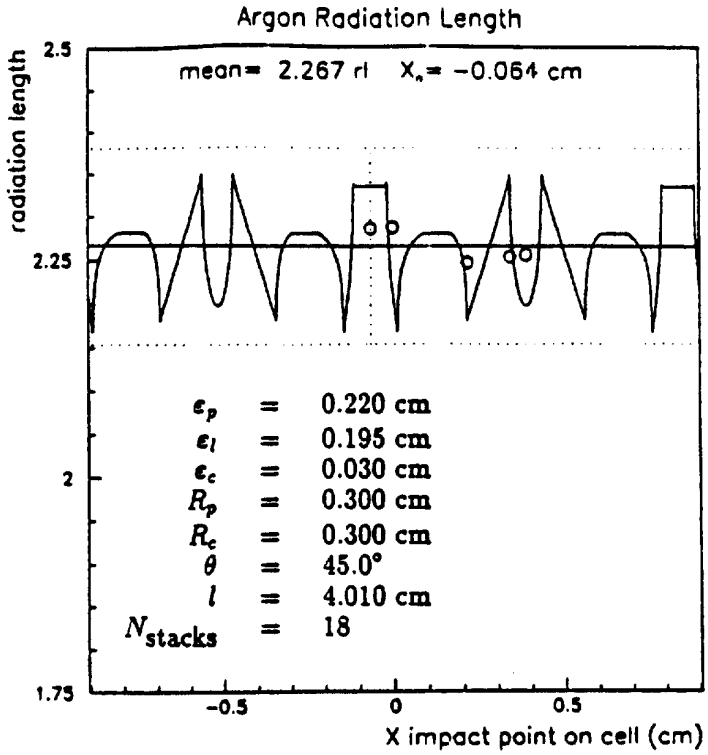

Figure 9: LAr radiation length traversed by a particle travelling along the Z axis as a function of its impact point X value for an optimum cell geometry. The horizontal dotted lines bound a ±5% band. The open circles show the response for 40 GeV electrons at normal incidence. The charge collection and readout are not simulated. The average response is made to coincide with the average LAr radiation length.

Geometry	X(cm)	μ(GeV)	σ(GeV)	α (% GeV$^{1/2}$)
optimum $\epsilon_l = 0.195$ cm	-0.064	6.950 ± 0.008	0.09 ± 0.01	8.2 ± 0.9
	0.	6.955 ± 0.007	0.09 ± 0.01	8.2 ± 0.9
	0.215	6.830 ± 0.008	0.09 ± 0.01	8.3 ± 0.9
	0.314	6.851 ± 0.007	0.09 ± 0.01	8.3 ± 0.9
	0.388	6.858 ± 0.007	0.08 ± 0.01	7.4 ± 0.9
non-optimum $\epsilon_l = 0.190$ cm	0.	6.833 ± 0.008	0.09 ± 0.01	8.3 ± 0.9
	0.250	6.686 ± 0.008	0.10 ± 0.01	9.5 ± 0.9
	0.402	6.650 ± 0.008	0.09 ± 0.01	8.6 ± 1.0
non-optimum $\epsilon_l = 0.200$ cm	0.	7.071 ± 0.008	0.10 ± 0.01	8.9 ± 0.9
	0.179	6.963 ± 0.009	0.10 ± 0.01	9.1 ± 0.9
	0.374	7.088 ± 0.008	0.09 ± 0.01	8.0 ± 0.9

Table 1: Simulation results for 40 GeV electrons at normal incidence. The charge collection and readout are not simulated. For a given geometry and impact point X the average (μ) and r.m.s. (σ) of $E_{\rm tot}$ are shown, along with the resolution coefficient α.

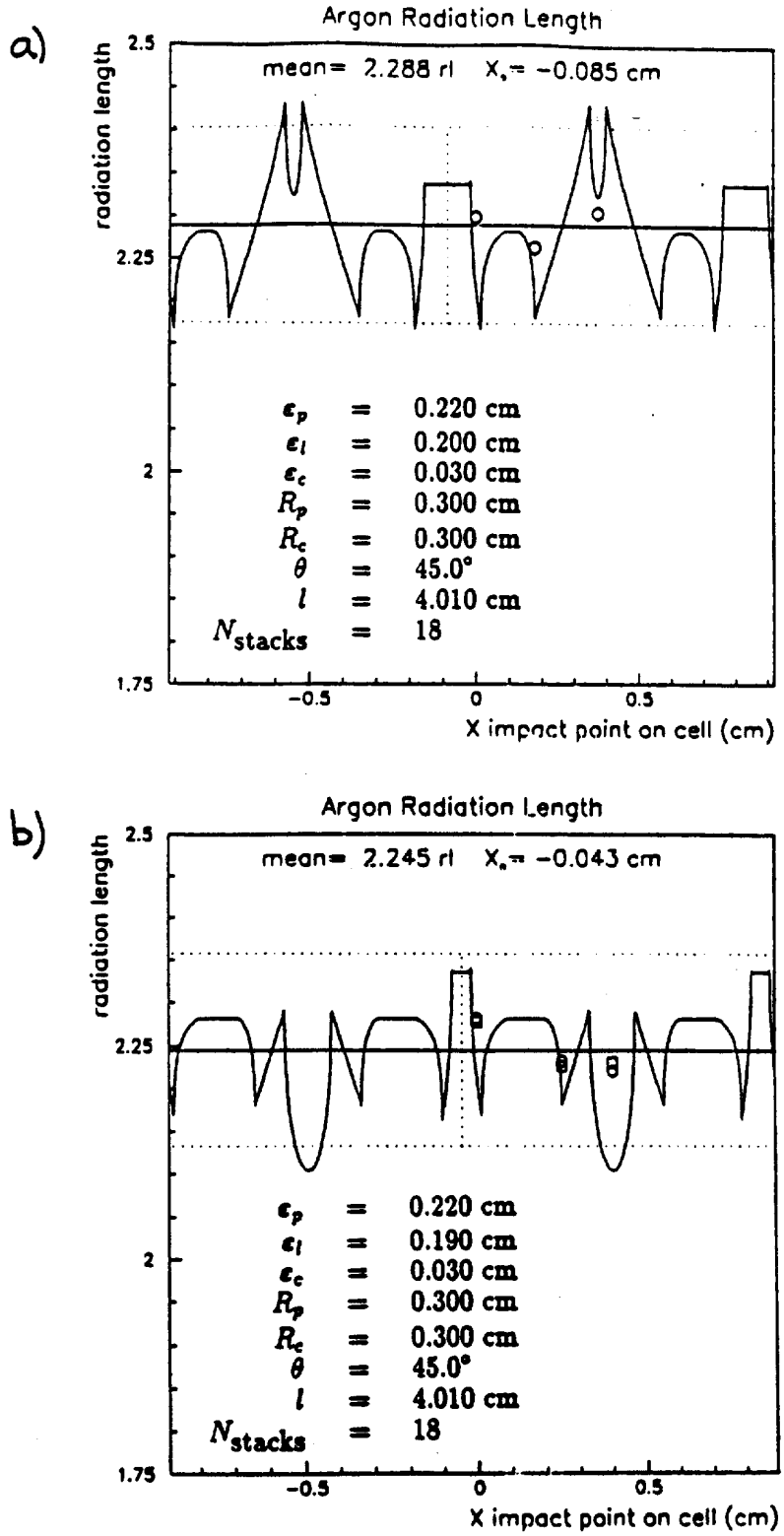

Figure 10: LAr radiation length traversed by a particle travelling along the Z axis as a function of its impact point X value for two non-optimum cell geometries. The horizontal dotted lines bound a ±5% band. The open circles show the response for 40 GeV electrons at normal incidence without the charge collection and readout simulation. The response corrected for charge collection and readout is shown by open squares. The average response is made to coincide with the average LAr radiation length.

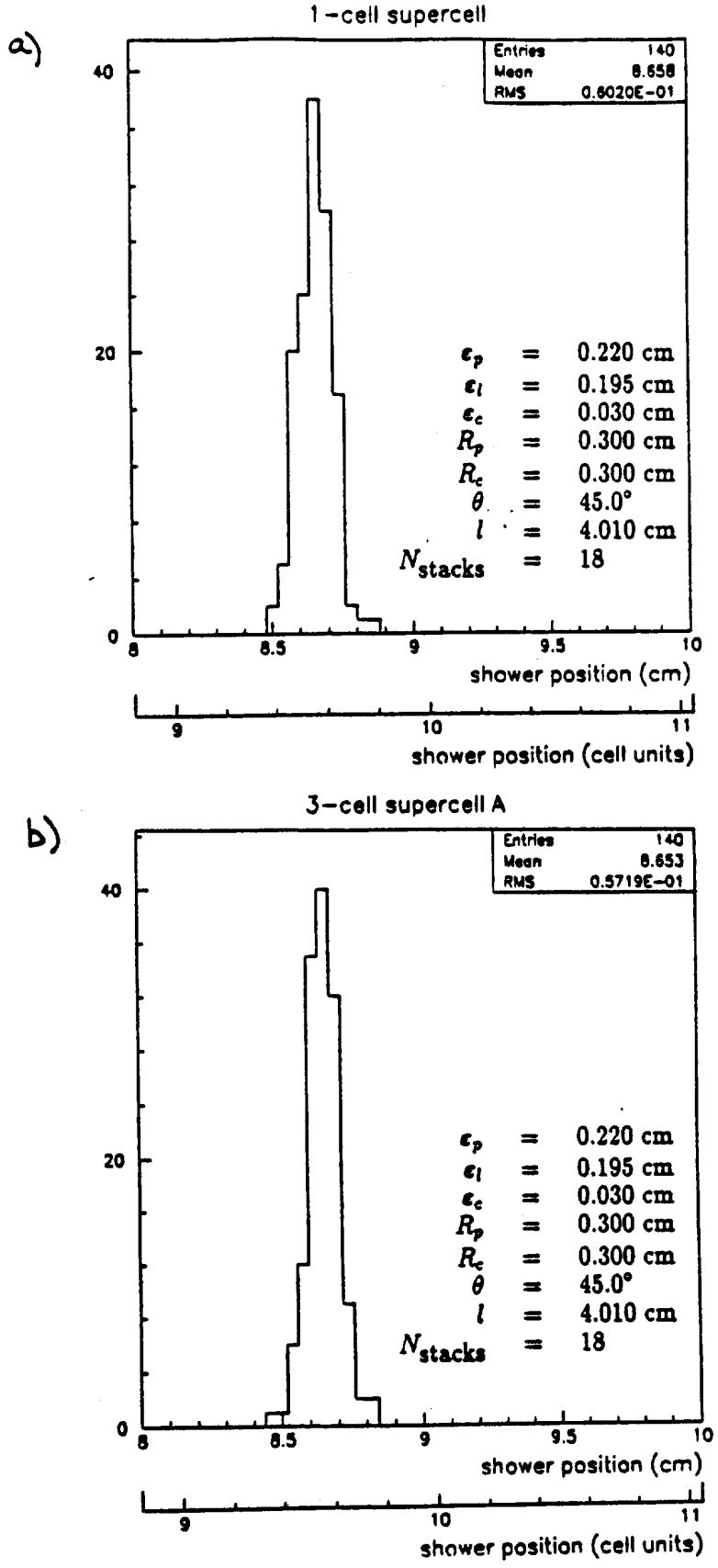

Figure 11: Distribution on the reconstructed position of 40 GeV electron showers impinging at normal incidence on the centre of a cell, for an optimum cell geometry. Supercells (see text) are composed of (a) one (b) three cells.

Geometry	X(cm)	μ^w(GeV)	σ^w(GeV)	α^w (% GeV$^{1/2}$)	σ^r/μ^r(%)
non-optimum	0.	5.891 ± 0.007	0.077 ± 0.009	8.3 ± 0.9	0.29 ± 0.03
$\epsilon_l = 0.190$ cm	0.250	5.756 ± 0.007	0.08 ± 0.01	8.8 ± 1.1	0.28 ± 0.03
	0.402	5.768 ± 0.006	0.077 ± 0.009	8.4 ± 1.0	0.29 ± 0.03

Table 2: Simulation results for 40 GeV electrons at normal incidence. The charge collection and readout are simulated. For a given impact point X the average (μ^w) and r.m.s. (σ^w) of E^W_{tot} are shown, along with the resolution coefficient α^w and σ^r/μ^r (see text).

over all stacks. Let k be the number of supercells and E_i the energy of supercell i summed over all stacks. An estimate of the electron impact point $\overline{x}$ can be obtained from

$$\overline{x} = \frac{\sum_{i=1}^{k} x_i E_i}{\sum_{i=1}^{k} E_i}$$

where x_i is the X position of the centre of supercell i on the face of the calorimeter. Figure 11(a) shows the distribution of $\overline{x}$ for supercells one cell wide. The electrons are incident in the centre of cell 11. This corresponds to $x = 9.956$ cm, since the cell thickness in X is $\epsilon/\sin\theta = 0.9051$ cm in this case. The reconstructed position is found to be 8.658 ± 0.005 cm which corresponds to $11 - 1.534$ cell units. An offset of $n/2$ cells is expected in the case of uniform energy deposition, where n is the number of cells traversed per stack ($n = 3$ in this case, see section 2.2). The corresponding electron position resolution is found to be 0.060 ± 0.007 cm.

Similar results are obtained in the case of supercells composed of 3 cells, as can be seen in Fig. 11(b).

5.2 Charge Collection and Readout Simulated

An electric field map was available for the non-optimum cell geometry shown in Figures 4(b) and 10(b). Charge collection and readout could therefore be simulated for various impact points. The response obtained is shown in figure 10(b) by open squares and in table 2. No significant effect is seen for the response uniformity.

To look for any degradation of resolution from the non-uniformity of the electric field and from the readout, let μ^w and σ^w be the average and r.m.s. of the E^W_{tot} distribution respectively. Then the resolution for a given impact point can be written

$$\left(\frac{\sigma^w}{\mu^w}\right)^2 = \left(\frac{\sigma}{\mu}\right)^2 + \left(\frac{\sigma^r}{\mu^r}\right)^2$$

where μ^r and σ^r are respectively the average and r.m.s. of the ratio

$$r \equiv \frac{E_{tot}}{E^W_{tot}}.$$

The term σ/μ is the contribution from the statistical nature of the electromagnetic shower, and σ^r/μ^r is the contribution from the charge collection and readout. Figure 12 shows the r distribution for a centre cell impact point.

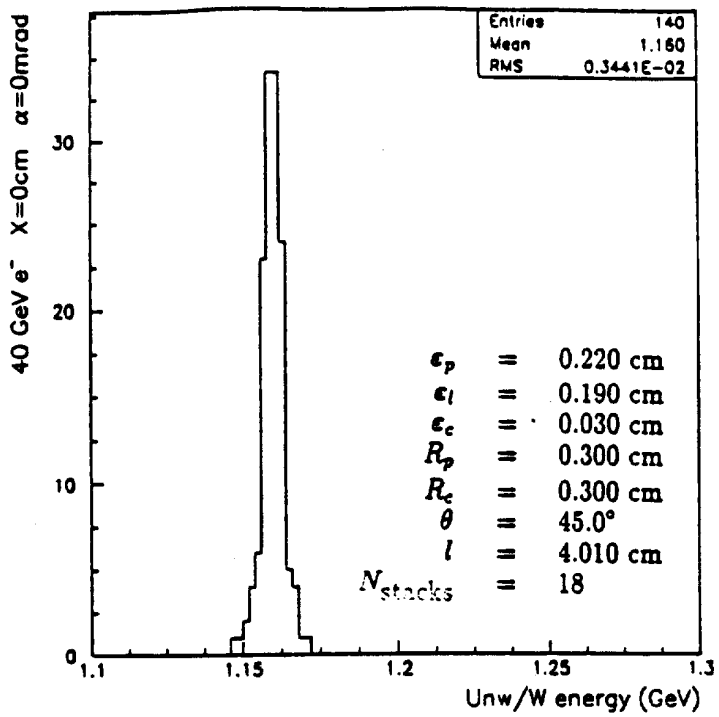

Figure 12: Distribution of the ratio r (see text) measured for a 40 GeV electron at normal incidence in the centre of a cell.

The results shown in table 2 give a contribution to the resolution from charge collection and readout of $\sigma^r/\mu^r = 0.29\%$. This value is expected to have a weak dependence on the energy of the electrons, as in the case of the 0.86 % contribution from the response non-uniformity mentioned in section 5.1. For comparison, the contribution to the resolution from the fluctuations of 40 GeV electromagnetic showers is found to be 1.3 % (see table 1). The contribution of the charge collection and readout to the resolution is therefore small (no electronic noise is simulated). Similar results are obtained for other impact points (see table 2).

6 PROTOTYPE CELL GEOMETRY

The final mechanical constraints for the construction of a prototype requires $\epsilon_c = 0.04$ cm. The final optimised geometry is shown in Fig 13.

7 CONCLUSIONS

A LAr calorimeter with accordion design (LAC) was geometrically described. Results from Monte Carlo simulations of 40 GeV electron showers were reported. Only electrons with normal incidence were treated.

It is found that the geometrical parameters of the LAC can be optimised by maximising the response uniformity for muons. Optimum parameters were obtained for the construction of a prototype.

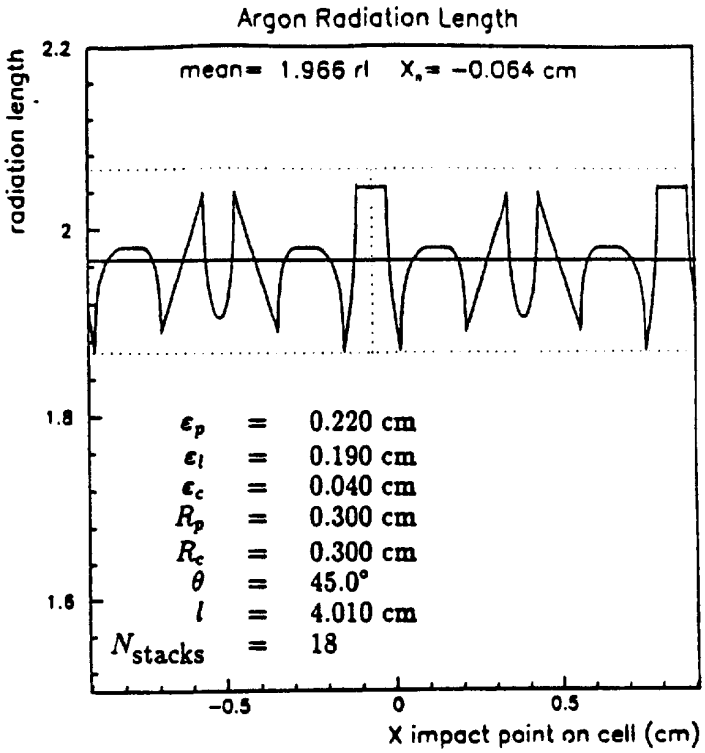

Figure 13: LAr radiation length traversed by a particle travelling along the Z axis as a function of its impact point X value for the final optimum cell geometry. The horizontal dotted lines bound a ±5% band.

The response non-uniformity for 40 Gev electrons is found to be 0.86 %. This contribution to the resolution is expected to have a weak dependence on energy, as for the contribution from charge collection (non-uniform electric field) and readout (without electronic noise) which is found to be 0.29 %.

These contributions to the resolution add quadratically to the intrinsic shower resolution, which is found to be 1.3% for 40 GeV electrons (resolution coefficient 8.2%). Preliminary results on the position resolution of 40 GeV electron showers give a resolution of approximately 0.06 cm.

Futur simulation plans include the study of the energy dependence of the response and resolution and their uniformity. Electromagnetic shower properties, such as leakage and size, and the angular resolution of their position reconstruction can also be studied. Further refinements in the readout simulation should include the simulation of electronic noise and readout threshold.

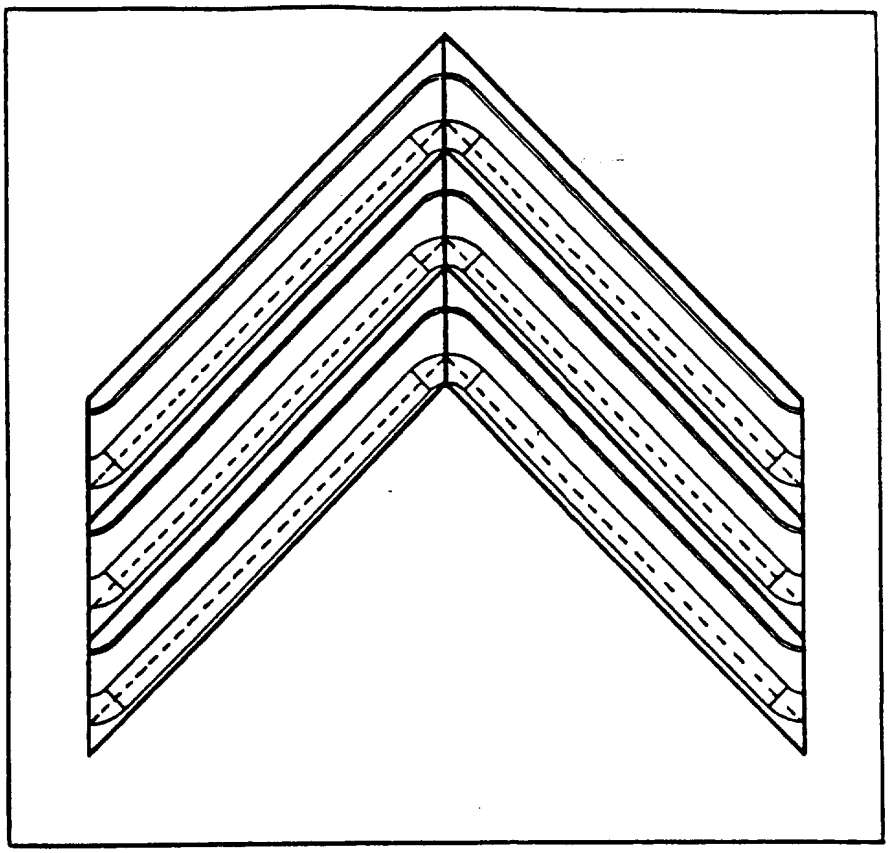

Figure 14: Software representation of the pseudocells (thick lines) and the cells (dashed lines).

A GEANT cell geometry

As it was pointed out in section 2, the LAr gaps shape is not part of GEANT volume repertoire. This problem is solved by considering pseudocells with boundaries in the LAr gaps. These pseudocells are filled with LAr; the lead and electrode sheets are then positioned in them. Pseudocells can be seen in Fig. 14. The cell divisions run parallel to the sheets, and join the inside of the lead sheet bends. The awkwardness of this artificial division is compensated by a big gain in computer time. The LAC coordinate system must also be adjusted in consequence. It is important to note that the division of the LAC in such pseudocells is possible only if

$$R_p + R_e < \frac{\epsilon_l}{1-\sin\theta} + \frac{\epsilon_p}{2} + \frac{\epsilon_e}{2}.$$

Any point in the LAC coordinate system, which is directly obtained from GEANT, can be translated into a cell number, a stack number and a position in the cell coordinate system. The position of the energy deposited by a charged track in the LAr in the cell coordinate system is then available, for example, to obtain the local value of the electric field. To obtain the cell number from a point in the LAr coordinate system, a line is drawn in the lead sheet, joining the outside of both bends, as shown in Fig. 14 by dashed lines. Such trick is geometrically allowed if

$$s - \left(R_p - \frac{\epsilon_p}{2}\right) \geq 0$$

where

$$s \equiv \frac{\sin\beta}{\sin\left(\frac{\pi}{2} - \beta + \theta\right)} \left(R_p + \frac{\epsilon_p}{2}\right)$$

and

$$\tan\beta \equiv l\sin\theta \left[l\cos\theta - 2R_p\left(\frac{1}{\sin\theta} - 1\right) + \epsilon_p\right]^{-1}.$$

B GEANT simulation parameters

The simulation of the passage of particles through the LAC is dependent on various GEANT parameters that control the physics processes simulated. In this study, the following datacards were used for the simulation of electrons:

```
DCAY 1
MULS 1
PFIS 1
MUNU 1
LOSS 1
PHOT 1
COMP 1
PAIR 1
BREM 1
DRAY 1
ANNI 1
HADR 1
```

All these datacards were set to zero for the simulation of minimum ionising muons, except `LOSS 1` and `DRAY 2`. This choice of datacards does not really simulate muons, but it was adequate for the study of the LAr radiation length traversed treated in section 2.2.

As mentioned in section 4.1, the cutoff energy for photons and electrons was set to 100 KeV and 1 MeV respectively:

```
CUTS 1=0.0001 2=0.001
```

Finally, the simulation also depends on the tracking medium parameters. The parameters of relevance here are the maximum displacement for multiple scattering in one tracking step (`DMAXMS` in cm), the maximum fractional energy loss in one step (`DEEMAX`), the tracking precision (`EPSIL` in cm) and the minimum tracking step due to energy loss or multiple scattering (`STMIN` in cm). In the case of vacuum, the medium parameters used were the following:

```
DMAXMS = 1.
DEEMAX = 0.5
EPSIL  = 0.0001
STMIN  = 0.2
```

For the other tracking media, the following parameters were used:

```
DMAXMS = 0.3
DEEMAX = 0.1
EPSIL  = 0.0001
STMIN  = 0.2
```

Whit these medium parameters, practically every GEANT hits are located on LAr gap boundaries, therefore minimising the number of hits.

C Interpolation in Electric Field and Weights Maps

A serious problem arises when the value of the electric field close to a LAr gap boundary is wanted, as the standard interpolation routine used [4] includes the field value zero in the interpolation. This produces the very bad effect that the field artificially goes to zero close to the LAr gap boundary. The same is true when interpolating in the weight map. In fact, when a dummy unit weight map is used, only about 85% of the total energy is obtained.

The standard interpolation routine used *extrapolates* when a value of the map outside its boundary is sought. The undesired interpolation with zero is eliminated if the field and weight maps are mapped to a space where the LAr gaps are rectangles. The interpolation or extrapolation is performed in this space. When a unit weight map is used in this way, all the total energy is recovered (to machine precision). The price to pay is a small distorsion due to the different densities in the Euclidean and in the interpolation spaces, as can be seen in Fig 15 where are shown the electric field strength and the electric field vector obtained from interpolating in the map shown in Fig. 5.

References

[1] The electric field map was provided by Pierre Petroff, Orsay group.

[2] M. Chen et al. : ECFA Study Week on Instrumentation Technology for High Luminosity Hadron Colliders, liquid detector working group, CERN 89-10, page 515, figure 5.

[3] V. Radeka, S. Rescia : Nucl. Instr. and Meth. **A265** (1988) 228.

[4] The interpolation routine used is FINT, CERN program library E104, KERNLIB.

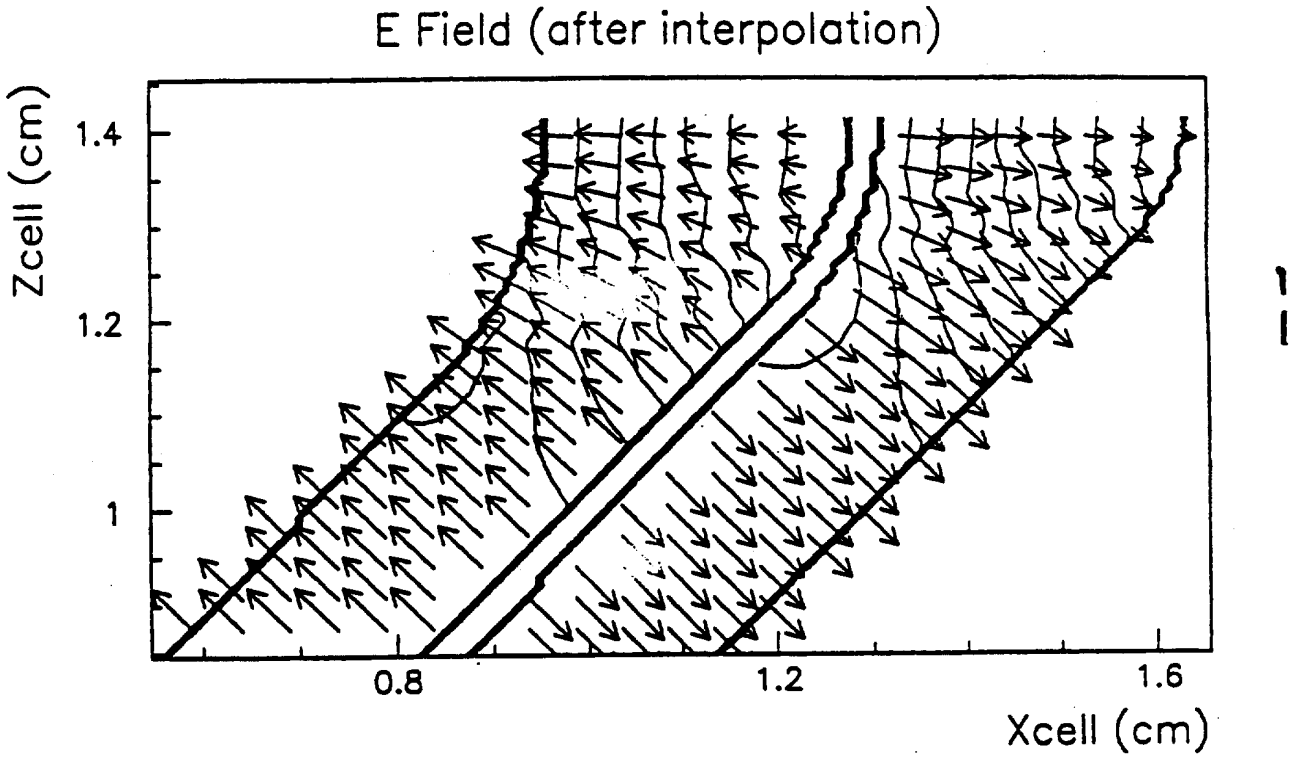

Figure 15: Electric field strength contours for the region of the LAr gaps close to a bend obtained after interpolation. The field vector is also shown.